

Multiphoton-pumped UV-Vis transient absorption spectroscopy of 2D materials: basic concepts and recent applications

Yuri D. Glinka^{1,2, a)}

¹*The institute of Optics, University of Rochester, Rochester, NY 14627, USA*

²*Institute of Physics, National Academy of Sciences of Ukraine, Kyiv 03028, Ukraine*

^{a)}Electronic mail: yuridglinka@yahoo.com

Abstract

2D materials are considered a key element in the development of next-generation electronics (nanoelectronics) due to their extreme thickness in the nanometer range and unique physical properties. The ultrafast dynamics of photoexcited carriers in such materials is strongly influenced by their interfaces, since the thickness of 2D materials is much smaller than the typical depth of light penetration into them and the mean free path of photoexcited carriers. The resulting collisions of photoexcited carriers with interfacial potential barriers of 2D materials in the presence of a strong laser field significantly alter the overall dynamics of photoexcitation, allowing laser light to be directly absorbed by carriers in the conduction/valence band through the inverse bremsstrahlung mechanism. The corresponding ultrafast carrier dynamics can be monitored using multiphoton-pumped UV-Vis transient absorption spectroscopy. In this review, we discuss the basic concepts and recent applications of this spectroscopy for a variety of 2D materials, including transition-metal dichalcogenide monolayers, topological insulators, and other 2D semiconductor structures.

1. Introduction

Since the discovery of the first single-layer material, graphene [1], the dynamics of ultrafast relaxation of photoexcited carriers in such a 2D material and a wide range of its single-layer analogues have been intensively studied using various pump-probe optical methods [2–30]. In general, 2D materials include graphene, boron nitride, transition-metal dichalcogenide monolayers, phosphorene, topological insulators (TI), 2D derivatives of the organic-inorganic hybrid perovskites, and other molecular systems including associated allotropes and compounds [1-30]. 2D materials are very promising for the next generation of electronics (nanoelectronics) due to their extreme thickness and unique physical properties. From an optical point of view, extreme thickness means that the depth of light penetration into such materials and the mean free path of photoexcited carriers significantly exceed their thickness [31-36]. This behavior expands the family of layered 2D materials to quasi-2D materials, such as single-layer 3D nanocrystals with a size range of several nanometers [37]. In most cases, 2D and quasi-2D materials and heterostructures based on them (for simplicity, below we will refer to all these structures as 2D materials) are grown or mechanically exfoliated from bulk crystals on transparent or opaque substrates, which are expected to play a significant role in the ultrafast dynamics of photoexcited carriers [6, 38-40].

One of the efficient methods for studying ultrafast carrier dynamics in 2D materials is transient absorption (TA) spectroscopy, implemented in transmission or reflection geometry [2-13, 24, 26-30, 37-40]. In the latter case, to switch to the absorption scale, the Kramers-Kronig transformation is necessary [10]. It is generally taken for granted that pumping in all TA experiments typically occurs in the one-photon absorption regime. Thus, as with all pump-probe experiments that used other non-optical probing methods such as angle-resolved photoemission, X-rays, and conductivity [14-23, 41, 42]. However, it has recently been shown that TA spectra of TI Bi₂Se₃ thin films extend to the entire visible

range and part of the UV range, although the energy of the pump photons lies in the IR range [24, 26, 28]. A similar spectroscopic upconversion was also observed for TA spectra of single-layer MAPbBr₃ nanocrystals [37], monolayers of transition-metal dichalcogenides [4-6, 10-12], and 2D selenium [43]. This behavior clearly indicates multiphoton absorption of pump photons even if the low pump fluences are used in TA experiments [26, 28]. Note here that although the term "low pump fluence" is widely used, it introduces confusion into nonlinear optics, since all nonlinear optical phenomena are uniquely determined by the light intensity (power density), and not by the light fluence (energy density). Therefore, a "low pump fluence" such as, for example, 100 μJ cm⁻² for 100 fs pulses corresponds to a pulse peak intensity of 1 GW cm⁻², which is more than sufficient to account for multiphoton excitation. Moreover, the shorter the femtosecond pulse, the higher the peak intensity, so it is quite surprising that multiphoton pumping in femtosecond TA spectroscopy of semiconductors was only recently discovered [26, 37].

However, since the energy of the pump photons exceeds the bandgap of the material or is in resonance with excitonic states, such a multiphoton process requires electrons (holes) in the conduction (valence) band or bound electron-hole pairs (excitons) to absorb the pump light upon excitation. Since the latter intraband process is not allowed in conventional bulk semiconductors due to restrictions on simultaneous conservation of energy and momentum [44], the mechanism of multiphoton pumping in 2D materials has been proposed as involving the absorption of light by free carriers via inverse bremsstrahlung [26-29, 37, 45]. Such a process requires consideration of collisions between free carriers and the interfacial potential barriers of 2D materials [46–48], a process that seems so natural in materials of this type. This mechanism is well known for impact and avalanche ionization below the femtosecond optical breakdown threshold in condensed matter, gases, and liquids [49, 50] and removes any restrictions on energy-momentum conservation for intraband optical transitions.

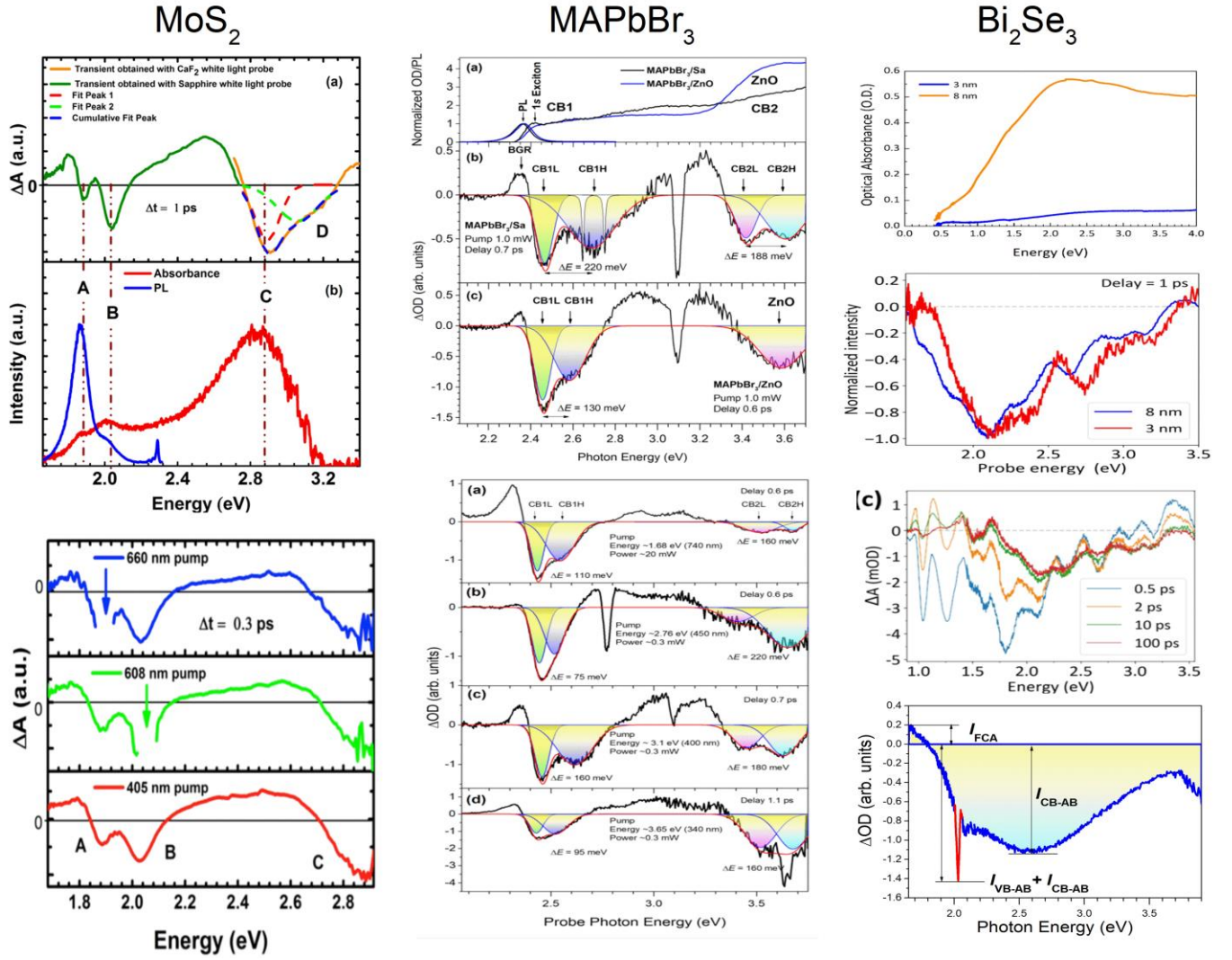


FIG. 1. Conventional absorption and transient absorption (TA) spectra of various 2D materials, as indicated at the top: left column – a monolayer of transition-metal dichalcogenide MoS₂, middle column – single-layer 20-nm-sized MAPbBr₃ nanocrystals, right column - 3D topological insulator Bi₂Se₃ with a thickness of 3 and 8 nm (first, second and third figures from top) and 10 nm (bottom figure). The left and middle columns also show the corresponding photoluminescence (PL) spectra as indicated, which were excited by photons with energies of 2.33 and 3.65 eV for MoS₂ and MAPbBr₃, respectively. For each TA spectrum shown in the left and middle columns, the pump photon energy at which it was measured is indicated. The TA spectra shown in the right column (second, third, and fourth from top) were measured at pump photon energies of 2.48 eV, 0.62 eV, and 2.07 eV, respectively. All TA spectra were measured at room temperature, except for the third one from the top in the right column, measured at 77 K. The figures in the left column are adapted from [4] [Copyright (2016) American Physical Society]. The figures in the middle column are adapted from [37]. The figures in the right column are adapted from [24], except for the bottom one, adapted from [45]. All figures in the middle and right columns are taken from publications licensed under CC-BY 4.0, except for the bottom one in the right column [Copyright (2023) IOP Publishing].

In this paper, we review experimental results on UV-Vis TA spectroscopy of several 2D materials for which TA spectra extend to energies well above the pump photon energy. We emphasize that this type of spectroscopic upconversion is associated with the dynamics of electrons initially excited by a multiphoton (multistep) process into high-energy states of the conduction band. The corresponding Pauli blocking within the electron relaxation dynamics provides the transient absorption bleaching, clearly manifested in the UV-Vis TA spectra [26-29, 37, 51-54]. The second contribution manifested in UV-Vis TA spectroscopy of 2D materials is the bandgap renormalization. This process mainly affects the band edge states, but its high-energy tail also overlaps with and significantly modifies the absorption bleaching peaks [37, 51-54]. We also consider all other effects that can appear in multiphoton-pumped UV-Vis TA spectroscopy of 2D materials,

such as inverse-bremsstrahlung-type free carrier absorption (FCA) [26, 28], valence band spin-orbit splitting due to the lack of inversion symmetry [4-8, 10-13, 55], and dynamic Rashba spin splitting of the conduction band induced by the built-in electric field [37]. We also emphasize that multiphoton pumping of carriers in 2D materials is due to collisional heating of electron-hole plasma caused by the inverse-bremsstrahlung-type FCA [26-29, 37, 45-47]. We compare this spectroscopy with two-photon photoemission spectroscopy (2PPES) of semiconductors [14-23, 56, 57] and multiphoton photoemission spectroscopy of noble metal surfaces [58-60]. Accordingly, we recognize that due to the band offsets at the interfaces of 2D materials [37, 61-63], absorption of pump photons by free electrons (holes) in the conduction (valence) band occurs because of collisions between free carriers and interfacial potential barriers [48]. Since this process is maximized at the peak

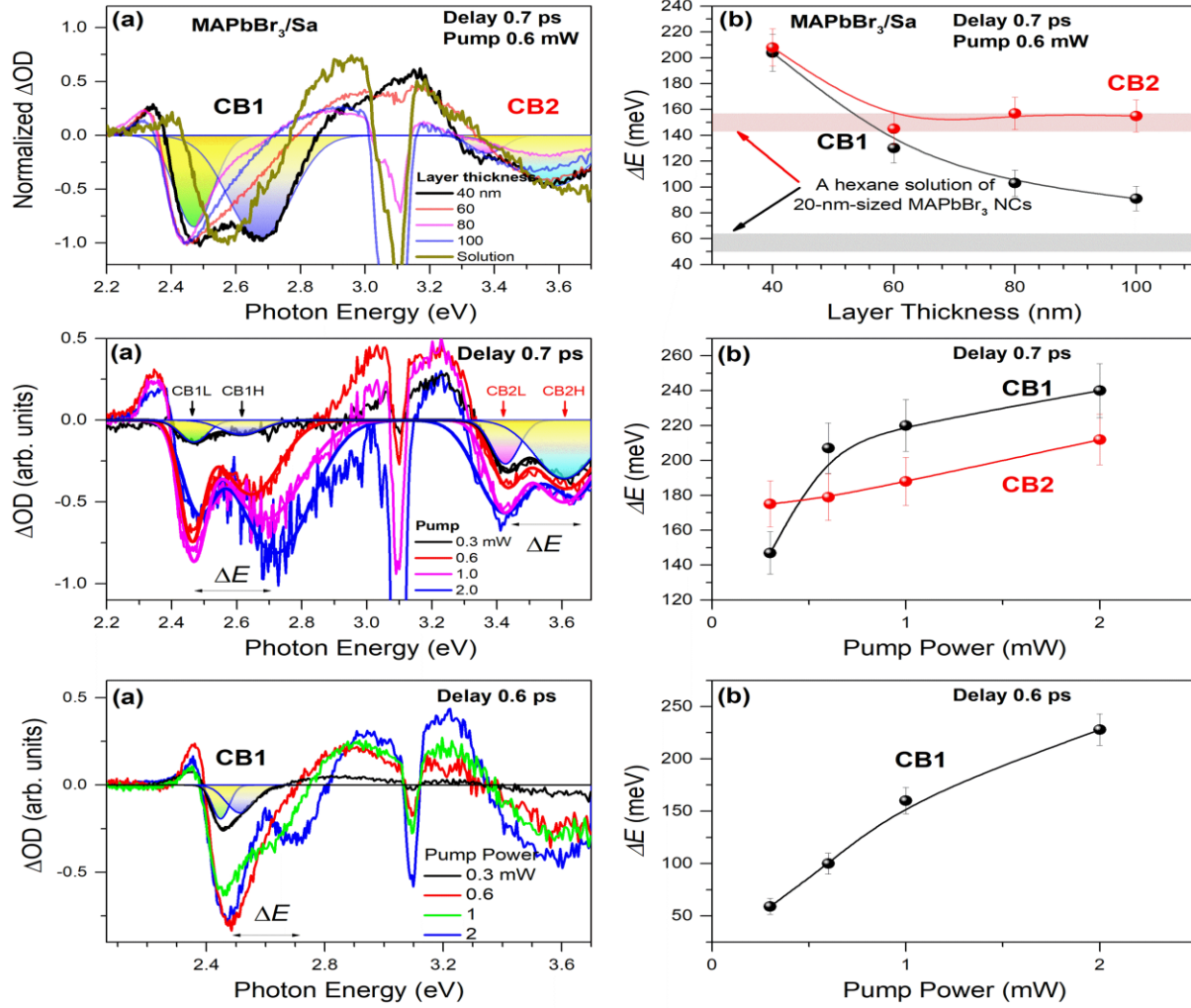


FIG. 2. Left column – The upper figure shows UV-Vis TA spectra of a hexane solution of MAPbBr₃ nanocrystals with a size of ~20 nm and a layer of MAPbBr₃ nanocrystals on a sapphire substrate with different layer thicknesses, as indicated by the corresponding colors. TA spectra were measured at ~0.7 ps delay using the ~3.1 eV pump photon energy and pump power of ~0.6 mW. The figures in the second and third rows show the TA spectra of MAPbBr₃ nanocrystals (layer thickness ~40 nm) on a sapphire and ZnO substrate, respectively, measured at the delay time as indicated, using pumping of ~3.1 eV of various powers, as indicated by the corresponding colors. Right column - the corresponding Rashba spin splitting energy (ΔE) as a function of layer thickness and pump power for the two conduction bands (CB1 and CB2) as indicated. All figures are adapted from [37], published under CC-BY 4.0 license.

intensity of the pump pulse, it precedes all carrier relaxation processes, including carrier-carrier thermalization, Auger heating and recombination, carrier multiplication, carrier-phonon scattering, and carrier recombination [26, 64-66]. Finally, we conclude that multiphoton-pumped UV-Vis TA spectroscopy most accurately accounts for the ultrafast dynamics of carriers in 2D materials, since it includes their collisions with interfaces.

2. UV-Vis TA spectra and band assignment

2.1. Typical UV-Vis TA spectra of 2D materials

Figure 1 compares conventional and transient absorption spectra of several 2D materials with different bandgap energies. If the bandgap energy of 2D materials lies in the visible range, as in a monolayer of MoS₂ and single-layer MAPbBr₃ nanocrystals, similar negative and positive features are observed in all TA spectra and their appearance is practically independent of the energy of

pump photons [4-6, 10-12, 37]. In general, the negative features are associated with absorption bleaching (a pump-induced decrease in absorption) [4-6, 10-12, 24, 26-29, 37, 51-54]. Since absorption bleaching contributions closely match all features of conventional absorption spectra, they correspond to the density of states of the conduction band of 2D materials and substrates (e.g., ZnO [37]) [26]. Consequently, the coincidence of spectral features in the conventional and transient absorption spectra clearly confirms that the negative peaks in the UV-Vis TA spectra are associated with carrier population dynamics. Despite the general similarity, the splitting of negative peaks has a different nature. In a monolayer of MoS₂, splitting manifests itself in the form of two types of excitons (usually denoted A and B), arising due to the lack of inversion symmetry in a monolayer system with strong spin-orbit coupling [55]. The resulting splitting (~160 meV) occurs at the maximum of the valence band [4-6, 10-12]. The higher energy peak also belongs to the exciton (usually denoted C), although it is separated from the A and B excitons by almost 1 eV and appears different.

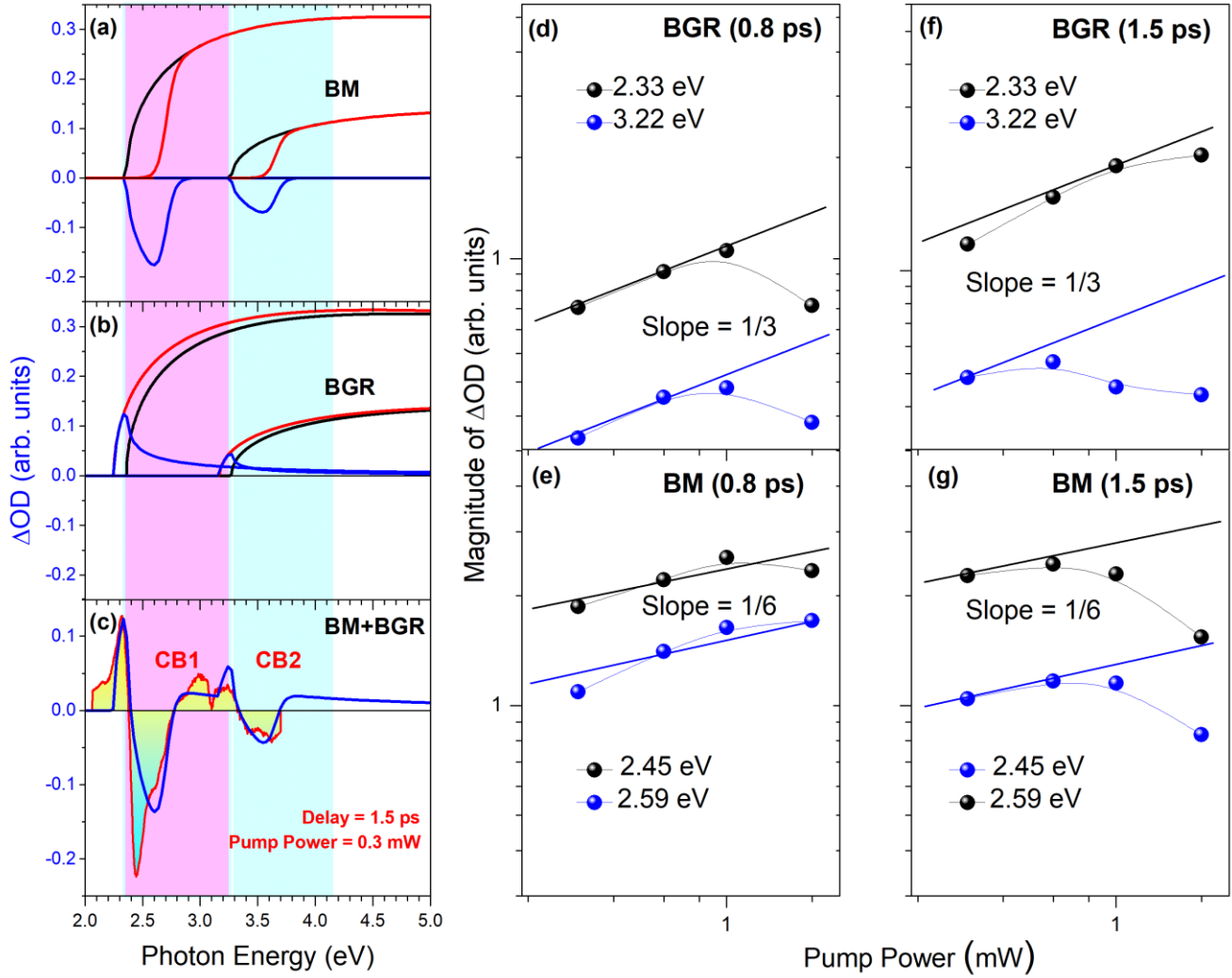


FIG. 3. [(a)–(c)] The numerical modeling of the Burstein-Moss (BM) and bandgap renormalization (BGR) contributions in UV-Vis TA spectra for two conduction bands (CB1 and CB2) of single-layer 20-nm-sized MAPbBr₃ nanocrystals. The black and red curves in (a) and (b) show the initial CB edge and that being modified by the photoexcited carrier population, respectively (the Rashba spin-splitting is ignored here), whereas the blue curves represent the difference between those two. The total effect (BM + BGR) is compared in (c) to the TA spectrum of single-layer MAPbBr₃ nanocrystals measured using ~ 3.1 eV pumping and parameters, as indicated. [(d)–(g)] The log-log plots of the pumping power dependences of the TA peak magnitudes (indicated by the corresponding colors), which were assigned to BM and BGR effects and measured at delay-times indicated in the corresponding brackets. The theoretically predicted slopes are shown as the straight solid lines. The figure is adopted from [37] published under CC-BY 4.0 license.

On the contrary, in single-layer MAPbBr₃ nanocrystals, the splitting, although of a similar magnitude, is associated with dynamic Rashba splitting of two conduction bands (CB1 and CB2) induced by the built-in electric field [37]. The development of the built-in electric field in 2D materials is initiated by the photo-Dember field arising from the instantaneous charge separation between photoexcited carriers. The latter assignment is clearly confirmed by the fact that the splitting magnitude strongly depends on the nature of the substrate, gradually increases with increasing pump power, and begins to appear and gradually increase as the thickness of the MAPbBr₃ nanocrystal layer approaches the single-layer limit (Fig. 2) [37].

The weaker positive contribution in UV-Vis TA spectra characterizes the pump-induced increase in absorption and is due to renormalization of the bandgap of 2D materials [10, 37, 51–54]. Although this effect is most pronounced in edge states, it is characterized by a high-energy tail that overlaps with the

absorption bleaching peaks, thereby providing positive contributions energetically located below and above them (Figure 3). The appearance of a broadband positive contribution to the UV-Vis TA spectra of 2D materials means that, in addition to renormalization of the bandgap, photoexcited carriers have an integral effect on the entire conduction band [37, 52].

If the bandgap energy of 2D materials lies in the IR range, for example, in TI Bi₂Se₃, then the broadband negative contribution to the UV-Vis TA spectra is also associated with absorption bleaching. Because this contribution in most cases follows the general smooth trend of conventional absorption spectra (Fig. 1, right column), it also corresponds to the density of states of the conduction band and therefore reflects the carrier population dynamics [26, 28, 45].

An additional positive feature of the UV-Vis TA spectra of 2D materials with bandgap energy in the IR range is related to the inverse-bremsstrahlung-type FCA (Fig. 1, right column). However, this effect is rarely observed, since the unique channel of carrier

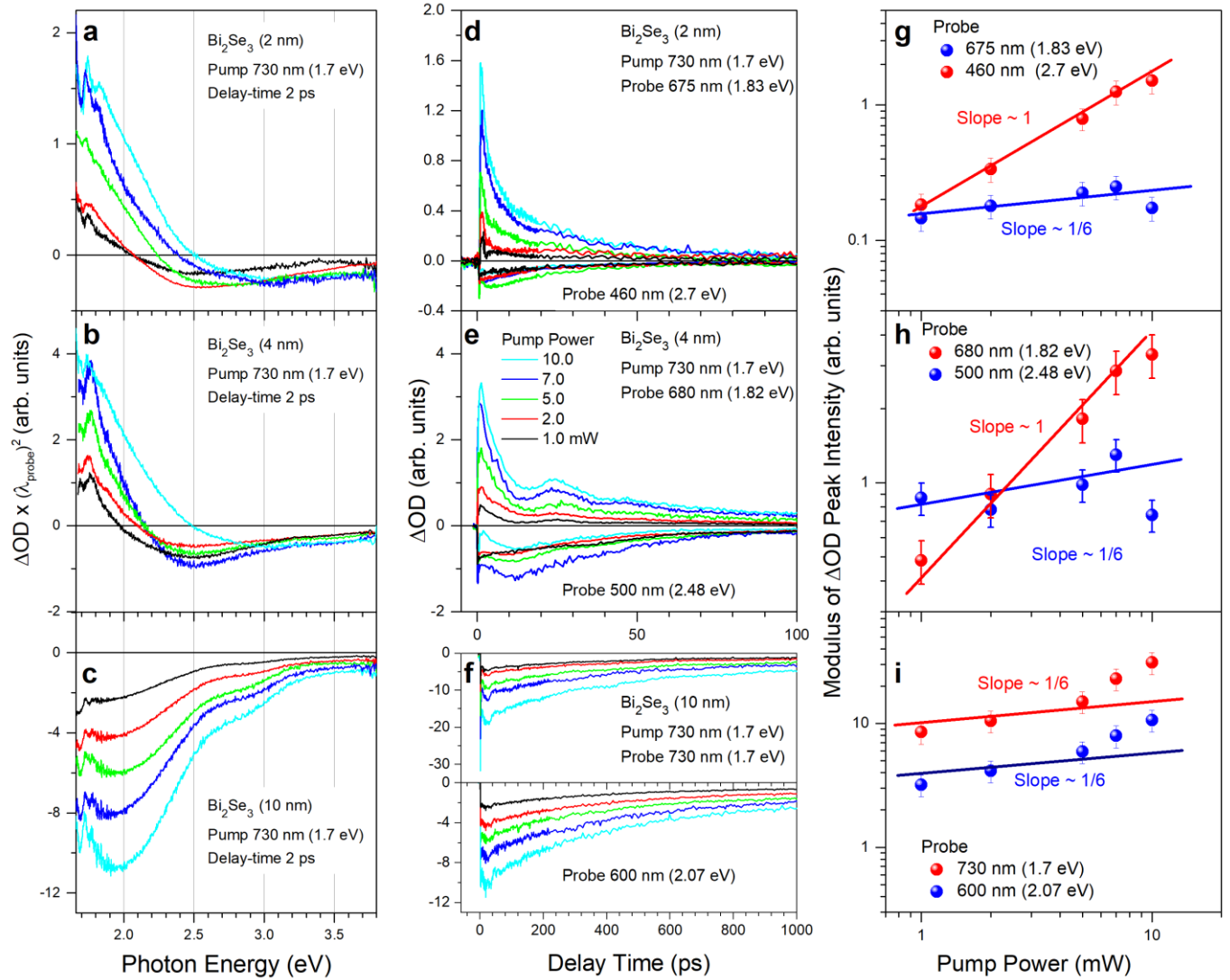


FIG. 4. (a–c) Set of UV-Vis TA spectra for Bi_2Se_3 films with various thicknesses, as indicated, measured at different pumping powers, as indicated by the corresponding colors. (d–f) Set of the corresponding pump-probe traces. All TA spectra and traces were measured under conditions indicated for each of the panels. (g–i) Power dependences of the modulus of the peak intensity of the pump-probe traces shown in (d), (e), and (f), respectively, which were plotted using log scales. The theoretically predicted slopes are shown by the corresponding color straight lines. The figure is adopted from [26] [Copyright (2021) American Chemical Society].

relaxation and a high spectral intensity of the supercontinuum probe beam are required, as was shown for 2D TI Bi_2Se_3 [26–29, 45].

2.2. Band assignment in the UV-Vis TA spectra

Thus, we have briefly discussed all the possible effects that can appear in the UV-Vis TA spectra of 2D materials and highlighted three unique contributions: absorption bleaching, bandgap renormalization, and inverse-bremsstrahlung-type FCA. We note here that these band assignments in the UV-Vis TA spectra of 2D materials are fundamentally different from those usually used for UV-Vis TA spectroscopy of chemical compounds and gas molecules. In the latter case, ground state bleaching, stimulated emission, excited state absorption, and product absorption are usually considered [67]. Correspondingly, in the Franck–Condon approximation, the intensity of the vibronic transition between the

ground and excited states (or between the excited and other excited states with higher energy) is proportional to the square of the overlap integral between the vibrational wave functions of the two states involved in the optical transition. Obviously, this approach and the terminology associated with localized molecular orbitals are not applicable to 2D semiconductors. The reason is that delocalized free carriers populate nearly continuous energy levels of the conduction/valence band according to the Fermi-Dirac distribution, including a variety of many-body effects such as correlated motion of carriers and their interactions with ionized impurities and lattice phonons [44, 48]. Therefore, UV-Vis TA spectroscopy of 2D materials should be considered within the framework of condensed matter physics. Despite the apparent obviousness of this statement, there are many publications in which the UV-Vis TA spectra of 2D materials are interpreted using models and terminology typically applied to chemical compounds and gas molecules. To be on the right track and avoid

terminological confusion, we note here in more detail the general trends in the ultrafast dynamics of carriers in 2D materials, including three main effects that could potentially contribute to their UV-Vis TA spectra.

2.2.1. Absorption bleaching.

The absorption bleaching process [also known as Burstein-Moss (BM) shift or Pauli blocking] dynamically expands the bandgap of a semiconductor by filling the conduction/valence band with photoexcited carriers [37, 51-54]. As mentioned in the previous section, this process is responsible for the negative contribution to the UV-Vis TA spectra. The initial population of carriers excited by a femtosecond pump pulse exists as an electron-hole plasma. Because plasma is neutral, it does not lead to any change in the complex refractive index of the materials and hence in their optical properties. Once the electron-hole plasma is thermalized due to carrier-carrier interactions, the carriers acquire their electron (hole) temperature causing the corresponding Fermi-Dirac distribution. The thermalization process results in the corresponding charge separation and typically manifests itself as a rise in the pump-probe signal. Further decay of the signal reflects the dynamics of cooling of pump-excited carriers, which occurs due to their inelastic scattering by LO phonons (Fröhlich relaxation mechanism) [26, 32, 37, 68-70]. The cooling dynamics are quite fast (<2 - 3 ps) and, in general, do not depend on the density of photoexcited carriers (n_e) [32, 37, 51-54]. Due to Pauli blocking, these relaxation dynamics, as well as the resulting accumulation of carriers at the edges of the conduction/valence band are imaged by the supercontinuum probe beam [4-6, 10-12, 24, 26, 28, 37, 45]. In general, this behavior manifests itself in a temporary redistribution of intensity within the absorption bleaching band of UV-Vis TA spectra towards lower energies [26, 37]. Consequently, the optical bandgap for the probe light appears to be dynamically expanded since the edge states become fully occupied (Fig. 3) [37, 51-54]. The peak amplitude of the absorption bleaching band weakly depends on the density of photoexcited carriers and scales as $n_e^{1/6}$ (Figs. 3, 4) [26, 28, 37].

2.2.2 Bandgap renormalization.

In addition to population dynamics, there is an integral influence of pump-excited carriers on the band structure of 2D materials, which manifests itself in a broadband positive contribution to the UV-Vis TA spectra. The broadband trend maximizing slightly below the bandgap energy indicates that new unoccupied states are generated by a shift of the entire conduction band (i.e., a rigid shift of the conduction band without changing the effective electron mass) (Fig. 3) [37, 52]. This behavior is due to many-body effects and leads to bandgap narrowing, which was originally associated with the bandgap renormalization (also known as bandgap shrinkage) [37, 51-54]. Figure 3(b) shows the effect for the trivial case of the density of states in the form of $(E - E_0)^{1/2}$ for the parabolic band [44], although the real shape of the high-energy tail of the positive contribution reflects all the features of the conduction band, including its nonparabolicity [37, 52]. The peak amplitude of the bandgap renormalization effect scales with the photoexcited carrier density as $n_e^{1/3}$ (Figs. 3 and 4) [26, 37, 52].

Thus, the mentioned effects of absorption bleaching, and bandgap renormalization completely control the optical bandgap of pumped 2D materials for probe light and therefore clearly appear in their UV-Vis TA spectra [4-6, 10-12, 26-29, 37, 45, 51- 54].

2.2.3 Free carrier absorption.

The most rarely observed contribution to the UV-Vis TA spectra of 2D materials is the absorption of light by free carriers. This effect provides another positive contribution to the UV-Vis TA spectra, in addition to the bandgap renormalization. The reason this behavior is so rarely observed is that free (non-interacting) electrons (holes) in the conduction (valence) band cannot be excited to higher energy band states by absorbing light (an intraband optical transition) due to restrictions on simultaneous conservation of energy and momentum [44]. However, there are two exceptions that allow absorbing light by free carriers. The first is associated with their collective excitation (spectral region below the plasma frequency - Drude-type FCA) [44]. The second exception is the absorption of light by free carriers when they collide with impurities, lattice defects or with interfacial potential barriers [48] (the spectral region above the plasma frequency - the inverse-bremsstrahlung-type FCA) [26-29, 37, 45-47]. Drude-type FCA for the UV-Vis spectral range can be neglected, since the plasma frequency even at high densities of photoexcited carriers in semiconductors ($\sim 10^{20}$ cm⁻³) lies in the IR spectral range [37, 44].

To observe the inverse-bremsstrahlung-type FCA, both a high density of photoexcited carriers and an intense probe laser beam ($\sim 10^{11}$ W cm⁻²) are required [49, 50]. Consequently, the reason that this process is rarely observed in UV-Vis TA spectroscopy of 2D semiconductors is that the spectral intensity of the supercontinuum probe beam is usually too low for the inverse bremsstrahlung process. Nevertheless, it was observed in the UV-Vis TA spectra of the topologically trivial phase of 2D TI Bi₂Se₃ (film thickness below 6 nm) (Fig. 4) [26, 28]. The observed exceptional behavior in the Dirac surface states is due to the dynamic accumulation of Dirac fermions in surface states and hence their direct interaction with the initial (unattenuated) intensity of the supercontinuum probe light. Note also that the peak amplitude of the positive contribution to the UV-Vis TA spectra due to the inverse-bremsstrahlung-type FCA is linearly dependent on the density of photoexcited carriers. As a result, this contribution can be easily distinguished from the positive contribution associated with the bandgap renormalization (Figs. 3 and 4).

3. Optimal experimental configuration

Compared with traditional optical spectroscopy, the overall performance of UV-Vis TA spectroscopy of 2D materials varies greatly depending on the actual design of the experimental setup and the angle of incidence of the pump and supercontinuum probe beams. Consequently, experimental results obtained by different research groups usually differ significantly from each other, not only due to differences in the quality of the samples, but also due to the actual design of the optical setup. It is worth noting that all commercially available TA spectrometers are usually designed for studying solutions of chemical compounds or nano/microcrystals. Since solutions are typically placed in a cuvette several millimeters thick, to maximize the amplitude of the pump-probe signal, it is necessary to increase the spatial overlap between the two focused beams. As a result, the angle between the pump and probe beams is usually set to a few degrees. In addition, due to the isotropy of solutions, the angle of incidence of the pump and probe beams is usually chosen arbitrarily. Obviously, such an experimental setup requires significant improvement for the study of 2D materials, usually presented in the form of thin films several nanometers thick.

3.1 Optimal experimental setup

The optimal experimental setup for UV-Vis TA spectroscopy of 2D materials appears to use normal incidence of the supercontinuum probe beam to avoid any material-related distortions [26-29, 37, 45]. This probe beam orientation is commonly used in all commercially available UV-Vis and IR absorption spectrometers. In addition, the angle of incidence of the pump beam must be large enough (30 - 45 degrees) to reduce the spatial overlap between the pump and probe beams. This arrangement will also make it possible to minimize the intensity of possible artifacts emanating from the substrate and to simplify the procedure for suppressing scattered pump light in the detection channel of the setup. The spot size of the probing beam should be $\sim 100 \mu\text{m}$, but at the same time 2-3 times smaller than the spot size of the pump beam, to avoid a discrepancy between the peak intensities of the pump and probe beams and to minimize the influence of material inhomogeneity. It should also be noted that the UV-Vis TA spectra obtained using transient reflection spectroscopy followed by Kramers-Kronig transformation are less accurate due to double-pass backscattering at the 2D-material-substrate interface. Therefore, preference is given to measuring the transmission of the probe light rather than its reflection.

3.2 Chirp correction

One of the fundamental problems of UV-Vis TA spectroscopy of 2D materials is that the TA spectra measured in the subpicosecond range are usually convolved with the chirp of the supercontinuum probe beam. Since UV-Vis TA spectra at this timescale characterize ultrafast carrier relaxation dynamics associated with the Fröhlich relaxation mechanism [26, 32, 37, 68-70], the chirp extraction procedure becomes extremely important to obtain accurate data. The chirp effect in commercially available TA spectrometers is usually minimized by using parabolic mirrors to collimate and focus the supercontinuum probe beam, as well as by optimizing the geometry of the experiment. However, the remaining chirp is still present, and its influence varies depending on the actual design of the experimental setup. This behavior means that the chirp of the supercontinuum probe beam must be measured and corrected numerically as part of a post-experimental procedure for each specific experimental setup. To measure the chirp effect, one can use degenerate four-wave mixing or two-photon absorption in the substrate measured at the same experimental conditions [28, 29, 71]. It is worth noting that incorrect chirp deconvolution often leads to the complete exclusion of the ultrafast relaxation stage associated with electron-phonon interaction from the UV-Vis TA spectra.

3.3 UV-Vis TA spectrum sign

In UV-Vis TA spectroscopy, probe light is pathing through the sample, and then collected and monitored using a spectrograph coupled with lock-in amplifier and CCD detector. Within this experimental configuration, the sign of the signal obtained by amplitude modulation of the pump beam can be easily switched to the opposite by changing the modulation phase of the lock-in amplifier by 180 degrees. Thus, the sign of TA spectra is ambiguous and must be chosen considering the nature of the physical process that causes the corresponding optical response. An incorrect choice of the sign of the UV-Vis TA spectrum will certainly lead to an incorrect interpretation of the experimental data.

4. The basic concepts of multiphoton-pumped UV-Vis TA spectroscopy

As we mentioned in Section 2.2.3, the inverse-bremsstrahlung-type FCA in UV-Vis TA spectra was observed only for 2D TI Bi_2Se_3 , since these materials exhibit a unique carrier relaxation channel through Dirac surface states. The main reason that this kind of absorption is rarely observed is apparently due to the rather low spectral intensity of the supercontinuum probing beam. However, this FCA mechanism can be very effective for a more intense narrowband pump beam. Since the amplitude of the inverse-bremsstrahlung-type FCA signal linearly depends on the density of photoexcited carriers and, therefore, on the pump power (Fig. 4) [26, 37, 47], the first-order optical process can be expected to dominate the pumping dynamics. In this regard, the inverse-bremsstrahlung-type FCA has been suggested to be the main phenomenon determining the implementation of multiphoton-pumped UV-Vis TA spectroscopy of 2D materials [26, 28, 37]. However, there are a few fundamental points that need to be clarified, as discussed below.

The pump regime in multiphoton-pumped UV-Vis TA spectroscopy of 2D materials largely corresponds to the regime in two-photon photoemission spectroscopy (2PPES) of semiconductors [14–23, 56, 57]. However, photoexcited electrons remain in the 2D material or are trapped at its interfaces rather than leaving the sample [26–29, 45]. Although 2PPES is usually associated with a two-photon process, it is more of a two-step process that uses a one-photon process at each step. In particular, the first photon creates a nonequilibrium distribution of electrons in the conduction band of a semiconductor, which is probed by the second photon through photoemission. The first process excites electrons from the valence band and is determined by the linear (first order) susceptibility of the material. In contrast, the second photon interacts with the electron gas and allows the photoexcited electrons to reach high-energy states of the continuum above the vacuum level. The interaction of a light pulse with the electron gas is also characterized by linear susceptibility, but of a completely different nature and scale. It is worth noting that despite the two-step nature of the 2PPE process, it can sometimes be characterized as a one-step process using effective second-order susceptibility [56]. However, this approach is in sharp contrast to traditional nonlinear optics, where the two-photon absorption process is characterized by third-order susceptibility [72, 73]. Moreover, the one-step approach in 2PPES is not justified if the sum frequency of the two photons is close to the plasmon resonance [56].

The high-energy continuum in 2PPES means that an electron with any crystal momentum can find a corresponding high-energy state and leave the crystal, after which it is selectively analyzed for its initial crystal momentum and energy using angle-resolved photoemission. With this experimental approach in 2PPES, simultaneous conservation of energy and momentum for optical transitions is always observed [57]. By introducing a delay between two light pulses, a time resolution in 2PPES is provided that allows the dynamics of photoexcited electrons to be studied with high precision [14-23, 56, 57]. Specifically, the combination of angular and time resolution in 2PPES allows one to study the time evolution of the energy distribution function (EDF) for a population of photoexcited electrons in the conduction band relative to their crystal momentum. Using this method, the dynamics of photoexcited electrons in the conduction band of 2D materials, as well as their remarkable features, have been studied [14–23].

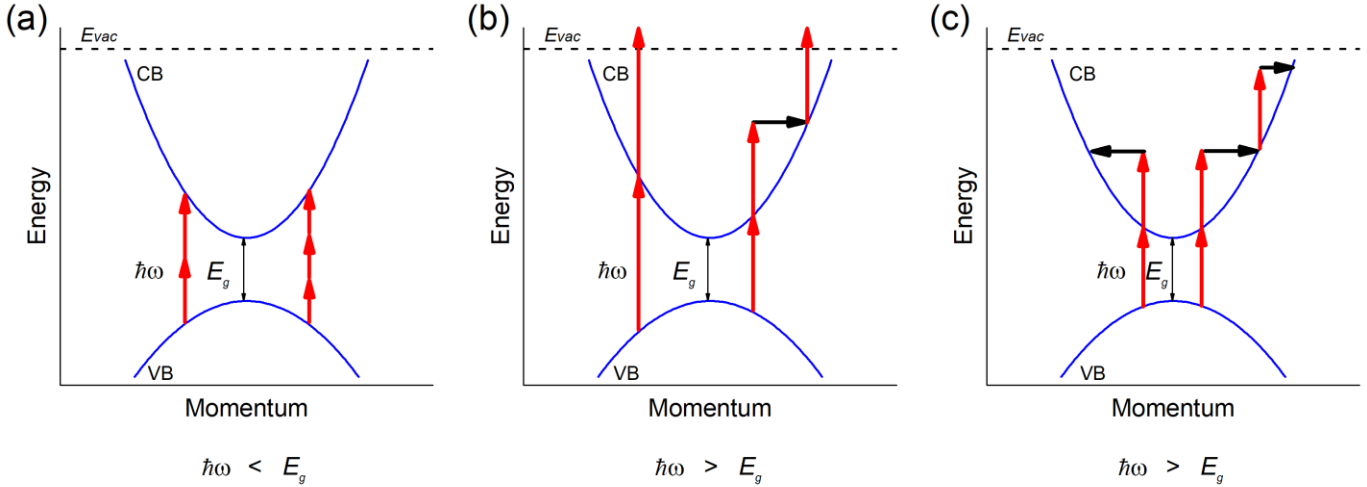


FIG. 5. (a) A schematic representation in energy-momentum space of two-photon and three-photon absorption processes with photon energy ($\hbar\omega$) below the bandgap energy (E_g) of the semiconductor. (b) and (c) A similar representation of two-step and three-step photoemission and absorption processes, respectively, with photon energies exceeding the semiconductor bandgap energy. E_{vac} represents the energy of the vacuum level. Collisions of photoexcited carriers with potential barriers at the interfaces of 2D materials, indicated by horizontal arrows, are required to simultaneously conserve energy and momentum for intraband optical transitions.

Thus, to create an electron gas in the conduction band of a semiconductor, the photon energy of the first laser pulse in 2PPES must always exceed its bandgap. The situation is completely different when the energy of the incident photon is less than the bandgap energy of the material. In the latter case, the excitation process can be exclusively multiphoton, when to bridge the valence and conduction bands it is necessary to simultaneously absorb several photons [Fig. 5(a)] [74-77]. Multiphoton absorption processes are characterized by high-order susceptibilities [72-77] and should therefore be distinguished from multi-step one-photon absorption processes, which are usually characterized by first-order susceptibilities at each step [37, 46, 47].

Unlike 2PPES, traditional pump-probe optical measurements non-selectively capture the influence of all possible elementary excitations in a semiconductor on its complex refractive index. This behavior leads to ambiguity in the interpretation of the results obtained. The situation can be significantly improved using UV-Vis TA spectroscopy [2-13, 24, 26-30, 37-40, 43, 45]. Despite the loss of electron momentum distribution, UV-Vis TA spectroscopy, like 2PPES, tracks population dynamics in the conduction band. Specifically, the time evolution of the EDF of photoexcited electrons can be monitored directly during their relaxation but using the Pauli blocking mechanism [26-29, 37]. Such population dynamics are well manifested, especially for high-energy states of the conduction band, where other mechanisms, such as bandgap renormalization, play a minor role [37].

However, it has recently been shown that the UV-Vis TA spectra of some 2D materials extend to energies significantly higher than the pump photon energy [4-6, 10-12, 24, 26, 28, 37, 43]. This kind of spectroscopic upconversion clearly indicates multiphoton absorption of pump photons [26, 28, 37]. Since the energy of the pump photons also exceeds the bandgap of the 2D material or is in resonance with the exciton states, such a multiphoton process requires electrons (holes) in the conduction (valence) band or excitons to absorb the pump photons upon excitation. However, due to restrictions on simultaneous conservation of energy and momentum for optical transitions,

direct absorption of light by an electron in the conduction band is allowed only when the final excitation step takes the electron into a high-energy continuum, as in 2PPES [Fig. 5(b)]. In other words, the electron must scatter its momentum to move to a higher energy state of the conduction band (an intraband optical transition) (Fig. 5) [44]. For this reason, multiphoton-pumped UV-Vis TA spectroscopy of conventional bulk semiconductors has never been considered.

The situation appears to be significantly different when electrons are excited in 2D materials. Since the depth of light penetration into such materials and the mean free path of photoexcited carriers significantly exceed the thickness of 2D materials [31-36], it can be expected that photoexcited carriers will experience collisions with interfacial potential barriers in the presence of a strong laser field [48]. The height of the potential barriers in 2D materials is determined by the band offsets at their interfaces [61-63]. The collision of electrons with potential barriers is confirmed by the fact that the energy of the electron after the absorption of a pump photon can exceed the height of the potential barrier, allowing the electron to be trapped at the interface [45]. If the carrier density is high enough and the laser light has sufficient power, collisions of electrons with interfacial potential barriers can remove any restrictions on energy-momentum conservation for intraband optical transitions. As a result, photoexcited electrons can be transferred to higher energy conduction band states [Fig. 5(c)]. This excitation mechanism is known as the inverse-bremsstrahlung-type FCA [26-29, 37, 45-47] and typically occurs during impact and avalanche ionization below the femtosecond optical breakdown threshold in condensed matter, gases, and liquids [49, 50].

Moreover, the inverse-bremsstrahlung-type FCA mechanism, in addition to the absorption mechanism occurring through intermediate resonances, is also responsible for heating the electron gas in metals [58-60]. It is well known that if the energy of an electron upon absorption of a photon exceeds the height of the potential barrier at the metal-medium interface, then the electron with some probability can be emitted from the metal [48]. As we

mentioned above, a similar type of electron dynamics has also been proposed for multiphoton-pumped UV-Vis TA spectroscopy of 2D materials, where electron trapping at interfaces is considered instead of photoemission [45]. Thus, inverse-bremsstrahlung-type FCA is the key process responsible for the nonequilibrium dynamics of multiphoton-pumped electron gas in electronic systems such as noble metals and topological insulators. Figure 5 compares in energy-momentum space all the mentioned electronic transitions associated with two- and three-photon absorption, two- and three-step photoemission, and two- and three-step absorption. These trends suggest vertical electronic transitions (Franck-Condon principle) and the inverse-bremsstrahlung-type FCA mechanism. It is worth noting that, despite the obvious multistep nature of the pumping process, we continue to call them multiphoton, like the two-photon (two-step) process in 2PPES.

Thus, collisional heating of photoexcited electron-hole plasma due to the inverse-bremsstrahlung-type FCA leads to multiphoton pumping of carriers in 2D materials to energies significantly exceeding the energy of pump photons. This process completely determines multiphoton-pumped UV-Vis TA spectroscopy of 2D materials. It is worth noting that the collisional heating model is ideally suited to the nature of 2D materials, since the frequency of collisions between free carriers and the interfacial potential barrier is expected to increase inversely with the thickness of 2D materials. To estimate the time between collisions, we use a 2D material thickness of ~ 1 nm and a maximum Fermi velocity of 10^6 m s⁻¹ [78]. The resulting value is 1 fs, a time that is well suited for the inverse-bremsstrahlung-type FCA in condensed matter [50].

This estimate implies that the collisional heating of carriers in 2D materials occurs within the pump pulse peak intensity. This behavior means that multiphoton excitation precedes all possible relaxation processes, including thermalization of carriers to electron (hole) temperature upon reaching the Fermi-Dirac distribution, Auger recombination and heating, carrier multiplication, electron-phonon scattering, and electron-hole recombination [26, 64-66]. A similar conclusion can be drawn regarding the observed dynamics of ultrafast relaxation of carriers through the split subbands. Both giant spin-orbit splitting in monolayers of transition-metal dichalcogenides [55] and dynamic Rashba splitting in single-layer MAPbBr₃ nanocrystals [37] affect the dynamics of carrier relaxation, but not the dynamics of their excitation. The lack of influence of the multiphoton pumping on all relaxation processes explains why UV-Vis TA spectroscopy with multiphoton pumping was not recognized in earlier experiments.

This behavior also means that there is no relaxation process that could be used to reveal the photonicity of the pump regime. As we noted in Sections 2.2.1 and 2.2.2, the pump power dependence of the peak intensity of the TA signals associated with absorption bleaching or bandgap renormalization also cannot be used to estimate the photonicity of multiphoton pumping. The reason is that the amplitude of these TA signals is not directly proportional to the density of photoexcited carriers [26, 28, 37, 52], as happens, for example, for photoluminescence (PL) signals [72-77]. Thus, the only evidence of multiphoton pumping in UV-Vis TA spectroscopy is the extension of the actual spectral range of probing towards energies exceeding the energy of pump photons. From this point of view, multiphoton-pumped UV-Vis TA spectroscopy is almost identical to one-photon-pumped TA spectroscopy, but with an extended range over which the ultrafast dynamics of photoexcited carriers can be studied. As an example, we can consider the dynamic Rashba splitting of the higher energy conduction band (CB2) in single-layer MAPbBr₃ nanocrystals,

which was observed in the energy region exceeding the energy of pump photons (Fig. 1) [37].

5. Recent applications of multiphoton-pumped UV-Vis TA spectroscopy

We are now reviewing several recent experimental observations for 2D materials that can be associated with multiphoton-pumped UV-Vis TA spectroscopy. Note that UV-Vis TA spectra extending to energies significantly higher than the energy of pump photons were first identified for single-layer MAPbBr₃ nanocrystals [37] and thin-film TI Bi₂Se₃ [26, 28]. The observed ultrafast dynamics of photoexcited electrons in these 2D materials is attributed to their multiphoton (two- or three-photon) pumping into high-energy states in the conduction band followed by relaxation. Moreover, it was concluded that the relaxation dynamics of photoexcited carriers under multiphoton pumping are very similar to the dynamics induced under one-photon pumping of the same energy [26-29]. This conclusion was also confirmed in the more recent application of multiphoton-pumped (three- to five-photon) UV-Vis TA spectroscopy to Bi₂Se₃ thin films [24]. These observations confirm the estimate made in the previous section that multiphoton pumping occurs within the peak intensity of the pump pulse and does not affect all possible relaxation processes.

Although similar spectroscopic upconversion has also been observed for some other 2D materials [4-6, 10-12, 24, 43], their UV-Vis TA spectra in the energy range exceeding the pump photon energy have not been explained as induced by multiphoton (multistep) pumping. Specifically, for MoS₂ monolayers, three negative peaks in the UV-Vis TA spectra were assigned to two spin-orbit split excitons at the band edges (A and B excitons) and a hot carrier exciton in the "band nesting" region (C exciton) [4, 5, 11-13]. The excitation of higher energy excitonic states (B and C excitons) when pumped into the lowest energy excitonic state (A exciton) is explained by the significant coupling between excitonic resonances in momentum space [4, 5]. However, the energy distance between excitons A and B, and A and C in MoS₂ monolayers is about 160 meV and 1 eV, respectively. Note that the latter value is more than twice the predicted maximum parameter for valence band splitting due to spin-orbit interaction [55]. Therefore, even if, due to some unique features of the band structure, this unimaginable coupling between exciton resonances A and B can be achieved, coupling between exciton resonances A and C (or B and C) seems very unlikely due to the extremely large energy mismatch.

In addition, we also draw attention to the fundamental difference between the UV-Vis TA spectra of a monolayer of MoS₂ and single-layer MAPbBr₃ nanocrystals, despite their overall similarity (Fig. 1). In particular, the decay traces of the three absorption bleaching peaks A, B and C in a MoS₂ monolayer show similar dynamics [4], suggesting that all types of excitons relax simultaneously at almost the same rates, despite the huge energy gap between them. In contrast, the decay traces of the higher energy split component in the UV-Vis TA spectra of single-layer MAPbBr₃ nanocrystals show a much shorter decay compared to the decay of the lowest energy component [37]. The latter behavior clearly demonstrates the general tendency of photoexcited carriers to relax into the lowest energy states at the band edges. However, such traditional relaxation dynamics do not appear in the UV-Vis TA spectra of a MoS₂ monolayer [4].

The discussed general trend of carrier relaxation is confirmed by the corresponding PL spectra. For both the MoS₂ monolayer and

single-layer MAPbBr₃ nanocrystals, the PL is dominated by recombination of the lowest energy excitons, despite their excitation through the higher energy states at 2.33 and 3.65 eV, respectively (Fig. 1). This behavior clearly indicates the relaxation of photoexcited carriers towards the lowest energy excitonic states. Thus, the unusual relaxation dynamics observed in the UV-Vis TA spectra of the MoS₂ monolayer contradicts the general trends of carrier relaxation in semiconductors. The identical relaxation dynamics observed in MoS₂ monolayers for A, B, and C excitons is most likely due to inappropriate experimental conditions or inaccurate post-experimental processing of UV-Vis TA spectra and chirp correction, as discussed in Section 3. For the same reason, the entire stage of ultrafast relaxation associated with electron-phonon scattering may be lost. This behavior is illustrated by the population of a higher energy exciton resonance (B) when pumped into a lower energy exciton resonance (A) and vice versa at zero delay, as observed in [10]. Obviously, this observation completely ignores any carrier population dynamics in the subpicosecond range.

Regarding exciton coupling, we note that the term “coupling between exciton resonances” is probably borrowed from coherent four-wave mixing spectroscopy of semiconductor quantum wells [79]. In these quantum systems, the splitting of excitonic states is too small (a few meV), so they are excited simultaneously within the laser pulse width. This behavior contrasts sharply with excitonic resonances observed for monolayers of transition-metal dichalcogenides, where, due to the large splitting energy, excitonic resonances are excited incoherently and independently. Accordingly, some complex models have been proposed to explain this unusual, highly energetic coupling between excitonic resonances [10, 12]. We also note that even in coherent spectroscopy of four-wave mixing of semiconductor quantum wells, there is no signal at zero delay, as presented in [10], and a certain delay between incident light pulses is necessary to populate excitonic resonances and observe the coherent coupling between them [79].

An alternative interpretation of the UV-Vis TA spectra of monolayers of transition-metal dichalcogenides can be proposed based on multiphoton pumping, as discussed above for other 2D materials [24, 26, 28, 37]. Accordingly, all contradictions in explaining the observed high-energy coupling between excitonic resonances can be eliminated. Following general trends, multiphoton-excited electrons and holes relax downward or instantaneously form excitons and then relax into band edge states depending on the exciton binding energy and the strength of the electron-phonon interaction. This Fröhlich relaxation mechanism of highly nonequilibrium carriers is also valid for monolayers of transition-metal dichalcogenides [68–70] and is generally accepted for polar III–V and II–VI quantum structures [80]. This model can explain all the above-discussed features of the dynamics of carrier relaxation in 2D materials, including monolayers of transition-metal dichalcogenides. Accordingly, through relaxation, multiphoton-pumped carriers populate all possible lower energy quantum states and excitonic states, as typically occurs in semiconductor quantum wells [80]. This mechanism does not require any coupling between such energetically distant exciton resonances in monolayers of transition-metal dichalcogenides. From this point of view, there is no difference between 2D materials and semiconductor quantum wells, except for the greater thickness and not so high potential barriers at the interfaces in the latter case.

Regarding the multiphoton-pumped UV-Vis TA spectra of TI Bi₂Se₃ thin films, we note that, despite the overall smooth trend of

conventional and transient absorption spectra, some internal structure of the broad absorption bleaching band can be observed (Fig. 1, right column). The internal structure is mainly observed in UV-Vis TA spectra measured at low temperatures, although it also appears slightly at room temperature [24]. In view of the above-mentioned trends in the splitting of the valence and conduction bands and the continuous density of states in them, such an internal structure of the absorption bleaching band seems unrealistic. Since the band structure and inhomogeneity of the sample do not change with temperature, the observed internal structure indicates the specifics of the experimental setup rather than a general trend with decreasing temperature. As discussed above in Section 3, UV-Vis TA spectroscopy is strongly influenced by the experimental conditions. Therefore, even the cryostat windows, their quality, and the angle of incidence of the laser beams on them can affect the final performance. In addition, proper post-experimental processing of UV-Vis TA spectra is critical to obtain accurate data.

The interpretation of the results of multiphoton (two- and three-photon) UV-Vis TA spectroscopy of 2D selenium also looks doubtful [43]. Specifically, the positive broadband contribution to the spectra was explained by absorption in the excited state. It is worth noting that such a positive broadband contribution has never been observed in UV-Vis TA spectra for any other 2D materials. Moreover, the approach and terminology used in [43] are usually applied to chemical compounds and gas molecules (Section 2.2). Since the absorption of light by electrons in the conduction band is allowed only as the inverse bremsstrahlung process (Section 4), the proposed interpretation of the UV-Vis TA spectra for 2D selenium seems questionable. On the other hand, if we assume that the sign of the contribution was incorrectly determined, as discussed in Section 3.2, then the opposite-sign UV-Vis TA spectra of 2D selenium accurately characterize the dynamics of absorption bleaching in this material. Thus, the resulting converted multiphoton-pumped UV-Vis TA spectra allow their interpretation for 2D selenium to be considered within the framework of generally accepted models for 2D materials (Section 2.2) and do not require any additional complex models, as discussed in [43].

Conclusions

In summary, we have reviewed experimental observations for several 2D materials in which UV-Vis TA spectra extend to energies well above the pump photon energy. This kind of spectroscopic upconversion is attributed to multiphoton (multistep) pumping in 2D materials caused by the inverse-bremsstrahlung-type free carrier absorption. This multiphoton excitation mechanism is due to collisional heating of the photoexcited electron-hole plasma within the peak intensity of the pump pulse. This behavior is due to the extreme thickness of 2D materials, which is much less than the typical depth of light penetration into materials and the mean free path of photoexcited carriers. It is concluded that multiphoton-pumped UV-Vis TA spectroscopy most accurately considers all the specific features of the ultrafast dynamics of carriers in 2D materials, since it includes their collisions with interfacial potential barriers. We also highlighted all the possible contributions to the UV-Vis TA spectra of 2D materials and considered them from the point of view of condensed matter physics. Specifically, we highlighted absorption bleaching, bandgap renormalization, and inverse-bremsstrahlung-type free carrier absorption. We also discussed the impact of valence and conduction band splitting dynamics, which typically occurs in 2D materials due to their 2D nature, on ultrafast carrier relaxation.

These dynamics clearly appear in multiphoton-pumped UV-Vis TA spectra and are associated with spin-orbit splitting of the valence band and dynamic Rashba spin splitting of the conduction band induced by the built-in electric field.

References

1. K. Novoselov, A. Geim, S. Morozov, *et al.* Two-dimensional gas of massless Dirac fermions in graphene. *Nature* **438**, 197–200 (2005).
2. L. Huang, G. V. Hartland, L.-Q. Chu, R. M. Feenstra, C. Lian, K. Tahy, H. Xing, Ultrafast transient absorption microscopy studies of carrier dynamics in epitaxial graphene, *Nano Letters*, **10** (4), 1308–1313 (2010).
3. S. Sharma, S. Liu, J. H. Edgar, I. Chatzakis, Auger recombination kinetics of the free carriers in hexagonal boron nitride, *ACS Photonics* **10** (10) 3586–3593 (2023).
4. S. H. Aleithan, M. Y. Livshits, S. Khadka, J. J. Rack, M. E. Kordesch, E. Stinaff, Broadband femtosecond transient absorption spectroscopy for a CVD MoS₂ monolayer, *Phys. Rev. B* **94**, 035445 (2016).
5. E. A. A. Pogna, M. Marsili, D. D. Fazio, S. D. Conte, C. Manzoni, D. Sangalli, D. Yoon, A. Lombardo, A. C. Ferrari, A. Marini, G. Cerullo, D. Prezzi, Photo-induced bandgap renormalization governs the ultrafast response of single-layer MoS₂, *ACS Nano*, **10**, 1182–1188 (2016).
6. P. Schiettecatte, P. Geiregat, Z. Hens, Ultrafast carrier dynamics in few-layer colloidal molybdenum disulfide probed by broadband transient absorption spectroscopy, *The Journal of Physical Chemistry C* **123** (16), 10571–10577 (2019).
7. Q. Cui, F. Ceballos, N. Kumar, H. Zhao, Transient absorption microscopy of monolayer and bulk WSe₂, *ACS Nano* **8** (3), 2970–2976 (2014).
8. X. Hong, J. Kim, S. F. Shi, *et al.* Ultrafast charge transfer in atomically thin MoS₂/WS₂ heterostructures. *Nat. Nanotech.* **9**, 682–686 (2014).
9. K. Zhang, B. Jin, C. Park, Y. Cho, X. Song, X. Shi, S. Zhang, W. Kim, H. Zeng, J. H. Park, Black phosphorene as a hole extraction layer boosting solar water splitting of oxygen evolution catalysts, *Nat. Commun.* **10**, 2001 (2019).
10. C. Trovatello, F. Katsch, Q. Li, X. Zhu, A. Knorr, G. Cerullo, S. Dal Conte, Disentangling many-body effects in the coherent optical response of 2D semiconductors, *Nano Letters*, **22**, 13, 5322–5329, (2022).
11. L. Yuan, T. Wang, T. Zhu, M. Zhou, L. Huang, Exciton dynamics, transport, and annihilation in atomically thin two-dimensional semiconductors, *The Journal of Physical Chemistry Letters*, **8** (14), 3371–3379 (2017).
12. L. Wang, Z. Wang, H.-Y. Wang, G. Grinblat, Y.-L. Huang, D. Wang, X.-H. Ye, X.-B. Li, Q. Bao, A.T.-S. Wee, S. A. Maier, Q.-D. Chen, M.-L. Zhong, C.-W. Qiu, H.-B. Sun, Slow cooling and efficient extraction of C-exciton hot carriers in MoS₂ monolayer, *Nat. Commun.* **8**, 13906 (2017).
13. W. Wang, N. Sui, Z. Kang, Q. Zhou, L. Li, X. Chi, H. Zhang, X. He, B. Zhao, Y. Wang, Cooling and diffusion characteristics of a hot carrier in the monolayer WS₂, *Optics Express*, **29**, 7736 (2021).
14. J. C. Johannsen, S. Ulstrup, F. Cilento, A. Crepaldi, M. Zacchigna, C. Cacho, I. C. E. Turcu, E. Springate, F. Fromm, C. Roidel, T. Seyller, F. Parmigiani, M. Grioni, P. Hofmann, Direct view on the ultrafast carrier dynamics in graphene, *Phys. Rev. Lett.*, **111**, 27403 (2013).
15. I. Gierz, J. C. Petersen, M. Mitran, C. Cacho, I. C. E. Turcu, E. Springate, A. Stöhr, A. Köhler, U. Starke, A. Cavalleri, *Nat. Mater.*, Snapshots of non-equilibrium Dirac carrier distributions in graphene, **12**, 1119–1124 (2013).
16. I. Gierz, S. Link, U. Starke and A. Cavalleri, Non-equilibrium Dirac carrier dynamics in graphene investigated with time- and angle-resolved photoemission spectroscopy, *Faraday Discuss.*, **171**, 311–321 (2014).
17. S. Ulstrup, J. C. Johannsen, F. Cilento, J. A. Miwa, A. Crepaldi, M. Zacchigna, C. Cacho, R. Chapman, E. Springate, S. Mammadov, F. Fromm, C. Roidel, T. Seyller, F. Parmigiani, M. Grioni, P. D. C. King, P. Hofmann, Ultrafast dynamics of massive Dirac fermions in bilayer graphene, *Phys. Rev. Lett.*, **112**, 257401 (2014).
18. F. Liu, Time- and angle-resolved photoemission spectroscopy (TR-ARPES) of TMDC monolayers and bilayers, *Chem. Sci.*, **14**, 736 (2023).
19. Y. H. Wang, D. Hsieh, E. J. Sie, H. Steinberg, D. R. Gardner, Y. S. Lee, P. Jarillo-Herrero, N. Gedik, Measurement of intrinsic Dirac fermion cooling on the surface of the topological insulator Bi₂Se₃ using time-resolved and angle-resolved photoemission spectroscopy. *Phys. Rev. Lett.* **109**, 127401 (2012).
20. J. A. Sobota, S.-L. Yang, D. Leuenberger, A. F. Kemper, J. G. Analytis, I. R. Fisher, P. S. Kirchmann, T. P. Devereaux, Z.-X. Shen, Distinguishing bulk and surface electron-phonon coupling in the topological insulator Bi₂Se₃ using time-resolved photoemission spectroscopy. *Phys. Rev. Lett.* **113**, 157401 (2014).
21. J. Gütde and U. Höfer, Ultrafast dynamics of photocurrents in surface states of three-dimensional topological insulators, *Phys. Status Solidi B*, **258**, 2000521 (2021).
22. M. Hajlaoui, *et al.* Tuning a Schottky barrier in a photoexcited topological insulator with transient Dirac cone electron-hole asymmetry. *Nat. Commun.* **5**, 3003 (2014).
23. S. Zhu, *et al.* Ultrafast electron dynamics at the Dirac node of the topological insulator Sb₂Te₃, *Sci. Rep.* **5**, 13213 (2015).
24. V. Campanari, D. Catone, P. O’Keeffe, A. Paladini, S. Turchini, F. Martelli, M. Salvato, N. Loudhaief, E. Campagna, P. Castrucci, Dynamics of the bulk-to-topological state scattering of photoexcited carriers in Bi₂Se₃ thin films, *ACS Appl. Electron. Mater.*, **5** (8) 4643–4649 (2023).
25. Y. D. Glinka, S. Babakiray, T. A. Johnson, M. B. Holcomb, D. Lederman, Nonlinear optical observation of coherent acoustic Dirac plasmons in thin-film topological insulators. *Nat. Commun.* **7**, 13054 (2016).
26. Y. D. Glinka, J. Li, T. He, X. W. Sun, Clarifying ultrafast carrier dynamics in ultrathin films of the topological insulator Bi₂Se₃ using transient absorption spectroscopy. *ACS Photonics* **8**, 1191 (2021).
27. Y. D. Glinka, T. He, X. W. Sun, Dynamic opening of a gap in Dirac surface states of the thin-film 3D topological insulator Bi₂Se₃ driven by the dynamic Rashba effect. *J. Phys. Chem. Lett.* **12**, 5593 (2021).
28. Y. D. Glinka, T. He, X. W. Sun, Two-photon IR pumped UV-Vis transient absorption spectroscopy of Dirac fermions in the topological insulator Bi₂Se₃. *J. Phys.: Condens. Matter* **34**, 465301 (2022).
29. Y. D. Glinka, T. He, X. W. Sun, Coherent surface-to-bulk vibrational coupling in the 2D topologically trivial insulator Bi₂Se₃ monitored by ultrafast transient absorption spectroscopy. *Sci. Rep.* **12**, 4722 (2022).
30. W. Lin, *et al.*, Combining two-photon photoemission and transient absorption spectroscopy to resolve hot carrier cooling in 2D perovskite single crystals: the effect of surface layer, *J. Mater. Chem. C*, **10**, 16751–16760 (2022).
31. S. Ki, M. Chen, X. Liang, Optoelectronic performance characterization of MoS₂ photodetectors for low frequency sensing applications, *J. Vac. Sci. Technol. B* **39**, 062201 (2021).
32. Y. D. Glinka, S. Babakiray, T. A. Johnson, A. D. Bristow, M. B. Holcomb, D. Lederman, Ultrafast carrier dynamics in thin-films of the topological insulator Bi₂Se₃. *Appl. Phys. Lett.* **103**, 151903 (2013).
33. F. Pizzocchero, L. Gammelgaard, B. Jessen, *et al.* The hot pick-up technique for batch assembly of van der Waals heterostructures. *Nat. Commun.* **7**, 11894 (2016).
34. R. Guo, X. Bu, S. Wang, G. Zhao, Enhanced electron-phonon scattering in Janus MoSSe, *New J. Phys.* **21**, 113040 (2019).
35. D. Wickramaratne, F. Zahid, R. K. Lake, Electronic and thermoelectric properties of few-layer transition metal dichalcogenides, *J. Chem. Phys.* **140**, 124710 (2014).
36. Y. Cai, J. Lan, G. Zhang, Y.-W. Zhang, Lattice vibrational modes and phonon thermal conductivity of monolayer MoS₂, *Phys. Rev. B* **89**, 035438 (2014).
37. Y. D. Glinka, R. Cai, J. Li, T. He, X. W. Sun, Observing dynamic and static Rashba effects in a thin layer of 3D hybrid perovskite nanocrystals using transient absorption spectroscopy. *AIP Adv.* **10**, 105034 (2020).
38. S. K. Saini, N. K. Tailor, P. Sharma, L. Tyagi, N. Vashistha, R. Yadav, A. K. Chaudhary, S. Satapathi, M. Kumar, Revealing the substrate

- dependent ultrafast phonon dynamics in Bi₂Se₃ thin films, *Adv. Mater. Interfaces*, **10** (3), 2201650 (2023).
39. Q. Liu, K. Wei, Y. Tang, Z. Xu, X. Cheng, T. Jiang, Visualizing hot-carrier expansion and cascaded transport in WS₂ by ultrafast transient absorption microscopy, *Adv. Sci.*, **9**, 2105746, (2022).
 40. F. Ahmad, R. Kumar, S. S. Kushvaha, M. Kumar, P. Kumar, Charge transfer induced symmetry breaking in GaN/Bi₂Se₃ topological heterostructure device, *npj 2D Materials and Applications*, **6**, 12 (2022).
 41. S. Kim, et al. Ultrafast carrier-lattice interactions and interlayer modulations of Bi₂Se₃ by x-ray free-electron laser diffraction *Nano Lett.* **21**, 8554 (2021).
 42. L. Luo, et al., Ultrafast manipulation of topologically enhanced surface transport driven by mid-infrared and terahertz pulses in Bi₂Se₃ *Nat. Commun.* **10**, 607 (2019).
 43. S. Prodhan, K. K. Chauhan, T. Singha, M. Karmakar, N. Maity, R. Nadarajan, P. Kumbhakar, C. S. Tiwary, A. K. Singh, M. M. Shaijumon, P. K. Datta, Comprehensive excited state carrier dynamics of 2D selenium: One-photon and multi-photon absorption regimes, *Appl. Phys. Lett.* **123**, 021105 (2023).
 44. P. Y. Yu and M. Cardona, *Fundamentals of Semiconductors: Physics and Materials Properties* (Springer, New York, 1996).
 45. Y. D. Glinka, T. He, X. W. Sun, Characterization of charge-carrier dynamics at the Bi₂Se₃/MgF₂ interface by multiphoton pumped UV-Vis transient absorption spectroscopy, *J. Phys.: Condens. Matter* **35**, 375301 (2023).
 46. V. R. Munirov and N. J. Fisch, Inverse Bremsstrahlung current drive, *Phys. Rev. E* **96**, 053211 (2017).
 47. R. Cauble and W. Rozmus, The inverse bremsstrahlung absorption coefficient in collisional plasmas, *Phys. Fluids* **28**, 3387 (1985).
 48. C. Kittel, *Introduction to solid state physics* (Wiley, 8th ed., 2004).
 49. C.A. Sacchi, Laser-induced electric breakdown in water, *J. Opt. Soc. Am. B* **8**, 337 (1991).
 50. A. Vogel, J. Noack, G. Huttman, G. Paltauf, Mechanisms of femtosecond laser nanosurgery of cells and tissue, *Appl. Phys. B* **81**, 1015–1047 (2005).
 51. J. P. Mondia, H. W. Tan, S. Linden, H. M. van Driel, J. F. Young, Ultrafast tuning of two-dimensional planar photonic-crystal waveguides via free-carrier injection and the optical Kerr effect, *J. Opt. Soc. Am.* **22**, 11 (2005).
 52. J. G. Lu, S. Fujita, T. Kawaharamura, H. Nishinaka, Y. Kamada, T. Ohshima, Z. Z. Ye, Y. J. Zeng, Y. Z. Zhang, L. P. Zhu, H. P. He, and B. H. Zhao, Carrier concentration dependence of band gap shift in n-type ZnO:Al films, *J. Appl. Phys.* **101**, 083705 (2007).
 53. Z. M. Gibbs, A. LaLonde, and G. J. Snyder, Optical band gap and the Burstein-Moss effect in iodine doped PbTe using diffuse reflectance infrared Fourier transform spectroscopy, *New J. Phys.* **15**, 075020 (2013).
 54. Z. Guo, Y. Wan, M. Yang, J. Snaider, K. Zhu, and L. Huang, Long-range hot-carrier transport in hybrid perovskites visualized by ultrafast microscopy, *Science* **356**, 59 (2017).
 55. Z. Y. Zhu, Y. C. Cheng, U. Schwingenschlögl, Giant spin-orbit-induced spin splitting in two-dimensional transition-metal dichalcogenide semiconductors, *Phys. Rev. B* **84**, 153402 (2011).
 56. C Timm and K H Bennemann, Response theory for time-resolved second-harmonic generation and two-photon photoemission, *J. Phys.: Condens. Matter* **16**, 661–694 (2004).
 57. H. Ohnishi and N. Tomita, Two topics of optical excitation dynamics, newly unveiled by the time- and momentum-resolved photo-electron emission from the conduction band of GaAs: A Theoretical Review, *Appl. Sci.*, **8**, 1788 (2018).
 58. M. Reutzler, A. Li, H. Petek, Above-threshold multiphoton photoemission from noble metal surfaces, *Phys. Rev. B* **101**, 075409 (2020).
 59. K. Cheng, J. Liu, K. Cao, L. Chen, Y. Zhang, Q. Jiang, D. Feng, S. Zhang, Z. Sun, T. Jia, Ultrafast dynamics of single-pulse femtosecond laser-induced periodic ripples on the surface of a gold film, *Phys. Rev. B* **98**, 184106 (2018).
 60. B. Rethfeld, A. Kaiser, M. Vicanek, G. Simon, Ultrafast dynamics of nonequilibrium electrons in metals under femtosecond laser irradiation, *Phys. Rev. B* **65**, 214303 (2002).
 61. S. K. Pradhan, B. Xiao, A. K. Pradhana, Energy band alignment of high-k oxide heterostructures at MoS₂/Al₂O₃ and MoS₂/ZrO₂ interfaces, *J. Appl. Phys.* **120**, 125305 (2016).
 62. D. Lizzit, P. Khakbaz, F. Driussi, M. Pala, D. Esseni, Ohmic behavior in metal contacts to n/p-type transition-metal dichalcogenides: Schottky versus tunneling barrier trade-off, *ACS Applied Nano Materials*, **6** (7), 5737-5746 (2023).
 63. Q. Zhang, S. Zhang, B. A. Sperling, et al. Band offset and electron affinity of monolayer MoSe₂ by internal photoemission. *J. Electron. Mater.* **48**, 6446–6450 (2019).
 64. M. Achermann, A. P. Bartko, J. A. Hollingsworth, V. I. Klimov, The effect of Auger heating on intraband carrier relaxation in semiconductor quantum rods, *Nat. Phys.* **2**, 557-561 (2006).
 65. C. M. Cirloganu, L. A. Padilha, Q. Lin, N. S. Makarov, K. A. Velizhanin, H. Luo, I. Robel, J. M. Pietryga, V. I. Klimov, Enhanced carrier multiplication in engineered quasi-type-II quantum dots, *Nat. Commun.* **5**, 4148 (2014).
 66. L. A. Padilha, J. T. Stewart, R. L. Sandberg, W. K. Bae, W.-K. Koh, J. M. Pietryga, V. I. Klimov, Aspect ratio dependence of Auger recombination and carrier multiplication in PbSe nanorods, *Nano Letters*, **13** (3), 1092-1099 (2013).
 67. R. Berera, R. van Grondelle, J. T. M. Kennis, Ultrafast transient absorption spectroscopy: principles and application to photosynthetic systems, *Photosynth. Res.* **101**, 105 (2009).
 68. K. Kaasbjerg, K. S. Bhargavi, S. S. Kubakaddi, Hot-electron cooling by acoustic and optical phonons in monolayers of MoS₂ and other transition metal dichalcogenides, *Phys. Rev. B* **90**, 165436 (2014).
 69. C. Ruppert, A. Chernikov, H. M. Hill, A. F. Rigosi, T. F. Heinz, The role of electronic and phononic excitation in the optical response of monolayer WS₂ after ultrafast excitation. *Nano. Lett.* **17**, 644–651 (2017).
 70. B. Miller, J. Lindlau, M. Bommert, A. Neumann, H. Yamaguchi, A. Holleitner, A. Högele, U. Wurstbauer, Tuning the Fröhlich exciton-phonon scattering in monolayer MoS₂, *Nat. Commun.* **10**, 807 (2019).
 71. V. I. Klimov and D. W. McBranch, Femtosecond high-sensitivity, chirp-free transient absorption spectroscopy using kilohertz lasers *Opt. Lett.* **23**, 277 (1998).
 72. Y. D. Glinka, R. Cai, X. Gao, D. Wu, R. Chen, and X. W. Sun, Structural phase transitions and photoluminescence mechanism in a layer of 3D hybrid perovskite nanocrystals, *AIP Adv.* **10**, 065028 (2020).
 73. R. W. Boyd, *Nonlinear Optics*, 3th ed. (Academic Press, Orlando, 2008).
 74. Y. D. Glinka, V. Y. Degoda, S. N. Naumenko, Multiphoton mechanism of generation of elementary excitations in disperse SiO₂, *Journal of non-crystalline solids*, **152**, 219-224 (1993).
 75. R. P. Chin, Y. R. Shen, V. Petrova-Koch, Photoluminescence from porous silicon by infrared multiphoton excitation, *Science* **270**, 776 (1995).
 76. Y. D. Glinka, K. W. Lin, S. H. Lin, Multiphoton-excited luminescence from diamond nanoparticles and an evolution to emission accompanying the laser vaporization process, *Appl. Phys. Lett.*, **74**, 236-238 (1999).
 77. Y. D. Glinka, S. H. Lin, Y. T. Chen, Two-photon-excited luminescence and defect formation in SiO₂ nanoparticles induced by 6.4-eV ArF laser light, *Phys. Rev. B* **62**, 4733 (2000).
 78. C. Hwang, D. Siegel, S. K. Mo, et al. Fermi velocity engineering in graphene by substrate modification. *Sci. Rep.* **2**, 590 (2012).
 79. Y. D. Glinka, Z. Sun, M. Erementchouk, M. N. Leuenberger, A. D. Bristow, S. T. Cundiff, A. S. Bracker, X. Li, Coherent coupling between exciton resonances governed by the disorder potential *Phys. Rev. B* **88** 075316 (2013).
 80. H. Zhao, S. Moehl, H. Kalt, Coherence length of excitons in a semiconductor quantum well. *Phys. Rev. Lett.* **89**, 097401 (2002).